Supersonic Jet," *Journal of Fluid Mechanics*, Vol. 51, Pt. 1, 1972, pp. 69–95.

[8] Bishop, K. A., Ffowcs Williams, J. E., and Smith, W., "On the Noise Sources of the Unsuppressed High-Speed Jet," *Journal of Fluid. Mechanics*, Vol. 50, Pt. 1, 1971, pp. 21–31.

[9] Dyer, I., "Distribution of Sound Sources in a Jet Stream," *The Journal of the Acoustical Society of America*, Vol. 31, No. 7, July 1959, pp. 1016–1022.

[10] Howes, W. L. and Mull, H. R., "Near Noise Field of a Jet Engine Exhaust. I. Sound Pressures," TN 3765, 1956, NACA.

[11] Maestrello, L. and McDaid, E., "Acoustic Characteristics of a High-Subsonic Jet," *AIAA Journal*, Vol. 9, No. 6, June 1971, pp. 1058–1066.

[12] Mollo-Christensen, E., "Jet Noise and Shear Flow Instability Seen from an Experimenter's Viewpoint," *Journal of Applied Mechanics*, March 1967, pp. 1–7.

[13] Morse, P. M. and Ingard, U. K., *Theoretical Acoustics*, McGraw-Hill, New York, 1968, pp. 717–727.

[14] Lange, F. H., *Correlation Techniques*, D. Van Nostrand, Princeton, N.J., 1967, pp. 167–168.

[15] Fisher, M. J. and Krause, F. R., "The Crossed-Beam Correlation Technique," *Journal of Fluid Mechanics*, Vol. 28, Pt. 4, pp. 705–717.

[16] Lighthill, M. J., "On Sound Generated Aerodynamically. I. General Theory," *Proceedings of the Royal Society*, A, Vol. 211, 1952, pp. 564–587.

[17] Ffowcs Williams, J. E., "The Noise from Turbulence Convected at High Speed," *Royal Society of London, Philosophical Transactions*, Series A, Vol. 255, 1962–63, pp. 469–502.

MAY 1974 AIAA JOURNAL VOL. 12, NO. 5

Method for Calculating Unsteady Turbulent Boundary Layers in Two- and Three-Dimensional Flows

ROBERT E. SINGLETON*
Army Research Office, Durham, N.C.
AND
JOHN F. NASH†
Scientific & Business Consultants, Inc., Atlanta, Ga.

The governing equations for an unsteady turbulent boundary layer on a swept infinite cylinder, composed of a continuity equation, a pair of momentum equations and a pair of rate equations for the shear stress, based on the turbulent kinetic-energy equation, are solved numerically. These rate equations for the shear stress express a balance between the convection, production, dissipation and diffusion of the turbulent shear stress components. Due to the physical model of turbulence employed, this system of equations is hyperbolic. An explicit, second-order accurate, conditionally stable difference scheme for this system, together with appropriate boundary and initial conditions, is formulated and developed into a computer program. Calculations for oscillating freestream flows with no pressure gradient show significant unsteady effects on the turbulent boundary layer. Expected phase shifts in wall shear stress and displacement thickness were found, as observed by other investigators. The quasi-steady wall shear stress values were a good approximation to the corresponding unsteady values for the entire frequency range considered. However, for these same frequency ranges, the same cannot be said of the displacement thickness values. The displacement thickness was not represented well by the quasi-steady model even at relatively low frequencies.

I. Introduction

THE role of unsteadiness, in many current fluid-mechanic problems, is of obvious importance, but at the same time, the subject of unsteady turbulent boundary layers has attracted few investigators. An important example of this situation is the flow over a helicopter rotor in translating motion. Preliminary investigations of this unsteady problem area[1] demonstrated the need to study the effects of time-dependence in rotor aerodynamics. Of course, dynamic stall affects, not only helicopter rotors, but also the blades of turbines and compressors, and the aerodynamic surfaces of maneuvering aerodynamic vehicles. Furthermore, the subject is of substantial fundamental interest, and a greater understanding of it would necessarily assist in the understanding of a much wider range of boundary-layer flows.

The subject of unsteady turbulent boundary layers is in its infancy. The differential method of Patel and Nash[2] and the integral method of McDonald and Shamroth[3] for calculating two-dimensional flows with both spatial and temporal variations were recently published. A few other methods have also appeared which treat only temporally-varying flows.[4,5]

The method presented in this paper is a further development of the method of Patel and Nash and an extension of their method to infinite-yawed-cylinder flows. A brief description is given of the governing equations, the turbulence model used and the necessary assumptions made. Details of the numerical method are described and illustrated by several example calculations,

Presented at the AIAA Computational Fluid Dynamics Conference, Palm Springs, Calif., July 19–20, 1973; submitted July 25, 1973; revision received November 26, 1973. This research was supported by Contract NAS2-6466 with the U.S. Army Air Mobility Research and Development Lab., Ames Research Center, Moffett Field, Calif.

Index categories: Boundary Layers and Convective Heat Transfer—Turbulent; Nonsteady Aerodynamics.

* Chief, Fluid Mechanics Branch.
† Staff.

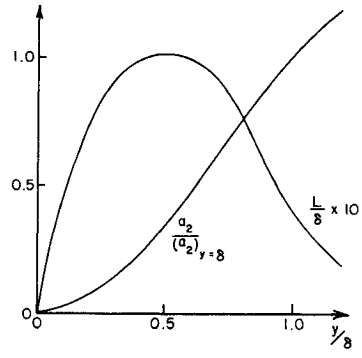

Fig. 1 Empirical functions.

which were made for simple unsteady freestream flowfields with no pressure gradient. Details of the flow physics and consequences of the assumptions which were made as well as detailed investigations of unsteady flowfields with several types of adverse pressure gradients are described in a companion paper, Ref. 6. Additional details relative to both of these papers are described in Ref. 7.

Even though a simple freestream flow was chosen to illustrate the application of the numerical method described in this paper, some interesting unsteady effects on the turbulent boundary layer were observed. Since time-dependent flowfield calculations are more difficult and expensive to perform than steady ones, it is helpful to know the point, in terms of increasing unsteadiness of the flow, beyond which the added complexity and expense have to be incurred in order to obtain useful results. The limited results given in this paper shed some light on this question.

II. Assumptions and Basic Equations

The method is designed to calculate a time-dependent, incompressible, turbulent boundary layer on an infinite yawed cylinder. Cartesian coordinates are placed on the surface of the cylinder (whose radius of curvature is assumed to be everywhere large compared with local boundary-layer thickness); x is measured normal to the generators, y normal to the surface, and z along the generators.

The velocities in the x-, y-, and z-directions are expressed in the form $U+u$, $V+v$, $W+w$, respectively, where U, V, W, u, v, w, are all functions of x, y, and t. Since the flow is assumed to be invariant in the direction parallel to the generators of the cylinder, the dependent variables are not functions of z. The components of velocity, $U(x, y, t)$, $V(x, y, t)$, $W(x, y, t)$, are defined as ensemble averages, taken over a large number of realizations of the same basic flow, or successive flows with the same time-history and the same boundary conditions, e.g., successive cycles of a stable oscillatory flow. The components, u, v, w, represent the random fluctuations about U, V, W, respectively, and by implication the ensemble averages of u, v, and w are identically zero.

The conservation of mass then takes the form

$$\partial U/\partial x+\partial V/\partial y = 0 \tag{1}$$

which can be immediately integrated to give V in quadrature form

$$V = -\int_0^y \frac{\partial U}{\partial x}\,dy \tag{2}$$

With the symbols, ρ, p, t, τ_x, τ_z, denoting the density, pressure, time, turbulent shear stress in x-direction, and turbulent shear stress in z-direction, respectively, and a superbar denoting ensemble averages, the conservation of momentum equations for the turbulent boundary layer, neglecting laminar shear stress, are

$$\frac{\partial U}{\partial t}+U\frac{\partial U}{\partial x}+V\frac{\partial U}{\partial y}+\frac{1}{\rho}\frac{dp}{dx}+\frac{\partial}{\partial y}\left(-\frac{\tau_x}{\rho}\right)=0 \tag{3}$$

$$\frac{\partial W}{\partial t}+U\frac{\partial W}{\partial x}+V\frac{\partial W}{\partial y}+\frac{\partial}{\partial y}\left(-\frac{\tau_z}{\rho}\right)=0 \tag{4}$$

where

$$\tau_x = -\rho\overline{uv},\quad \tau_z = -\rho\overline{vw}$$

The turbulent shear stresses are assumed to behave according to the rate equations used in the method for steady three-dimensional flows,[8,9] but with the convective derivative extended to include the time derivative

$$\frac{\partial}{\partial t}(\overline{uv})+U\frac{\partial}{\partial x}(\overline{uv})+V\frac{\partial}{\partial y}(\overline{uv})+2a_1\left[(\overline{uv}^2+\overline{vw}^2)^{1/2}\frac{\partial U}{\partial y}+\Phi_x+\frac{\partial}{\partial y}(a_2\overline{uv})+\frac{\overline{uv}}{L}(\overline{uv}^2+\overline{vw}^2)^{1/4}\right]=0 \tag{5}$$

$$\frac{\partial}{\partial t}(\overline{vw})+U\frac{\partial}{\partial x}(\overline{vw})+V\frac{\partial}{\partial y}(\overline{vw})+2a_1\left[(\overline{uv}^2+\overline{vw}^2)^{1/2}\frac{\partial W}{\partial y}+\Phi_z+\frac{\partial}{\partial y}(a_2\overline{vw})+\frac{\overline{vw}}{L}(\overline{uv}^2+\overline{vw}^2)^{1/4}\right]=0 \tag{6}$$

In this pair of rate equations the terms Φ_x and Φ_z are given by

$$\Phi_x = \Gamma\left[(\overline{uv}^2+\overline{vw}^2)^{1/2}\frac{\partial U}{\partial y}+\overline{uv}\left\{\left(\frac{\partial U}{\partial y}\right)^2+\left(\frac{\partial W}{\partial y}\right)^2\right\}^{1/2}\right]$$

$$\Phi_z = \Gamma\left[(\overline{uv}^2+\overline{vw}^2)^{1/2}\frac{\partial W}{\partial y}+\overline{vw}\left\{\left(\frac{\partial U}{\partial y}\right)^2+\left(\frac{\partial W}{\partial y}\right)^2\right\}^{1/2}\right]$$

and Γ is some large number (from experience, any number greater than about 4). Use of these expressions for Φ_x and Φ_z leads to codirectionality of the shear stress "vector" and rate of strain vector. The assumption of codirectionality can be relaxed, if desired, by putting

$$\Phi_x = \Phi_z = 0$$

The empirical functions, a_1, a_2, and L are assumed to be the same functions as appear in the steady-flow method[8,9]; a_2 and L are shown in Fig. 1, and $a_1 = 0.15$.

III. Numerical Method

Since turbulent boundary layers may grow (or diminish) rapidly with both increasing x and/or t, the numerical computation domain must reflect this reality. Thus a transformation

$$\begin{aligned} t &= t^* \\ x &= \xi \\ y &= S(x,t)\eta^\beta \end{aligned} \tag{7}$$

is introduced where β is a constant greater than unity, and S is the height of the computation domain. S is allowed to increase (or decrease) in sympathy with the boundary-layer thickness, $\delta(x,t)$, and an approximate proportionality is maintained between them. This proportionality cannot be made exact in an explicit scheme since the value of dS/dt must be assigned before $d\delta/dt$ is known. S is taken to be about 1.25δ. Primary mesh points lie on curves of constant y/S, and are distributed non-uniformly over the height of the domain to produce an increased density of points near the surface as illustrated in Fig. 2. If the points are distributed such that y_i is proportional to $(i-1)^\beta$, the transformation, Eq. (7), will transform the domain into one of constant thickness and uniform η-step.

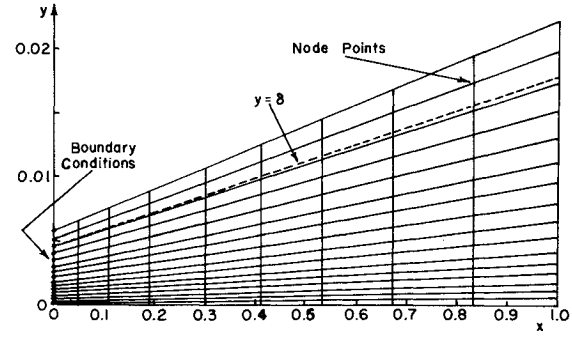

Fig. 2 Section x-y of the integration domain for a typical calculation.

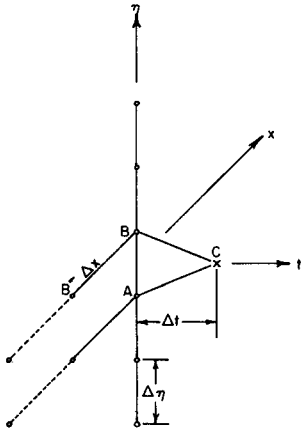

Fig. 3 Finite-difference molecule.

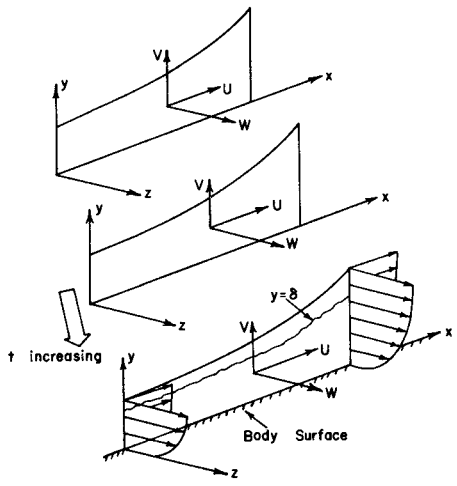

Fig. 4 Schematic representation of the method of calculation.

Having made the transformation, Eq. (7), and defining the vectors, F, C, and matrices, A, B, by

$$F=\begin{bmatrix} U \\ W \\ \overline{uv} \\ \overline{vw} \end{bmatrix},\quad C=\begin{bmatrix} c_1 \\ c_2 \\ c_3 \\ c_4 \end{bmatrix},\quad A=\begin{bmatrix} a_{11} & 0 & a_{13} & 0 \\ 0 & a_{22} & 0 & a_{24} \\ a_{31} & 0 & a_{33} & 0 \\ 0 & a_{42} & 0 & a_{44} \end{bmatrix}$$

$$B=\begin{bmatrix} b_{11} & 0 & 0 & 0 \\ 0 & b_{22} & 0 & 0 \\ 0 & 0 & b_{33} & 0 \\ 0 & 0 & 0 & b_{44} \end{bmatrix}$$

the governing equations take the form

$$\partial F/\partial t = A(\partial F/\partial \eta)+B(\partial F/\partial x)+C \tag{8}$$

where the $a_{i,j}$'s, $b_{i,j}$'s, c_i's ($i=1,\ldots,4$; $j=1,\ldots,4$) are functions of the dependent variables and the c_i's ($i=1,\ldots,4$), in addition, contain the terms in Φ_x, Φ_z which are nonlinear in the η-derivatives of U and W. The system of equations, Eq. (8), is hyperbolic, and is integrated in a three-dimensional domain (x, η, t) by means of an explicit, second-order accurate, staggered mesh, finite-difference scheme. The finite-difference molecule is shown in Fig. 3, and the scheme is given by

$$F_C=\frac{1}{2}(F_A+F_B)+\frac{1}{8}\Delta\eta\left[\left(\frac{\partial F}{\partial \eta}\right)_A-\left(\frac{\partial F}{\partial \eta}\right)_B\right]+\frac{1}{2}\Delta t\left[\left(\frac{\partial F}{\partial t}\right)_A+\left(\frac{\partial F}{\partial t}\right)_B\right] \tag{9}$$

This scheme has been shown by Nash[10] to be both second-order accurate and conditionally stable. A fourth-order accurate difference formula is used for the $\partial/\partial\eta$

$$\Delta\eta(\partial F/\partial\eta)_i=\tfrac{1}{12}F_{i-2}-\tfrac{2}{3}F_{i-1}+\tfrac{2}{3}F_{i+1}-\tfrac{1}{12}F_{i+2} \tag{10}$$

where the subscript i denotes the value of $F(\eta=\eta_i)$ and

$$\eta_i=(i-1)/(n-1)$$

where n = total number of mesh points across boundary layer.

Equation (10) cannot be used for $i=n-1$ and in this case, it is replaced by the third-order accurate scheme

$$\Delta\eta(\partial F/\partial\eta)_{n-1}=\tfrac{1}{6}F_{n-3}-F_{n-2}+\tfrac{1}{2}F_{n-1}+\tfrac{1}{3}F_n$$

The derivatives of the dependent variables with respect to x are discretized by either first or second-order accurate backward differences depending on the boundary-layer growth and mesh point distribution in the x-direction.

Boundary conditions for the calculation consist of

a) initial profiles of U, W, $\overline{uv}$, $\overline{vw}$ vs y for $t=0$ and all x;

b) initial profiles of U, W, $\overline{uv}$, $\overline{vw}$ vs y for $x=0$ and all t;

c) $\partial U/\partial y=\partial W/\partial y=\partial\overline{uv}/\partial y=\partial\overline{vw}/\partial y=0$; and $\overline{uv}=\overline{vw}=0$ at $y=1.25\delta$, 1.25δ being the local height of the integration domain, which varied with both x and t.

d) appropriate boundary conditions at $y=0$.

Because of the neglect of the laminar counterparts of the shear stress, the method cannot be extended to $y=0$ but must be matched to an approximate solution, at $y/\delta=0.05$, taken to be a generalized version of Townsend's inner law,[11] with modifications which permit departures from collateral flow through this inner layer, and which also permit small deviations from the strict linearity of the variation of shear stress with y.

The method then proceeds by first evaluating all the dependent variables over successive planes, $t=$ const, and advancing in the t-direction as illustrated in Fig. 4. The maximum permissible t-step is dictated by stability considerations. In the t-η plane, an examination of the angles of the characteristics shows that if

$$\Delta t \leqq [\eta^{\beta-1}/(a_1\tau_x)^{1/2}]\beta S\Delta\eta \tag{11}$$

then the scheme does not step outside the region covered by the "region of influence" of the initial data line AB. The term $(a_1\tau_x)^{1/2}$ will be recognized as an approximation to the tangent of the characteristic angle in two dimensions; the maximum value of this angle, in the outer layer, nearly always occurs at the matching station. In addition, a second check is made on Δt by application of the Courant-Friedrichs-Levy condition in the t-x plane,

$$\Delta t \leqq \Delta x/U \tag{12}$$

Hence, the t-step in most situations, is proportional to the smallest value of δ at the particular t-station, usually $\delta_{x=0}$. Figure 5 shows some typical run times on a UNIVAC 1106 computer as a function of $\delta_{x=0}$. It is seen that computation time varies inversely as the thickness of the upstream boundary layer. For most calculations done in this paper, $\delta_{x=0}$ was taken to be 0.00444, giving a typical computation of about 5 min.

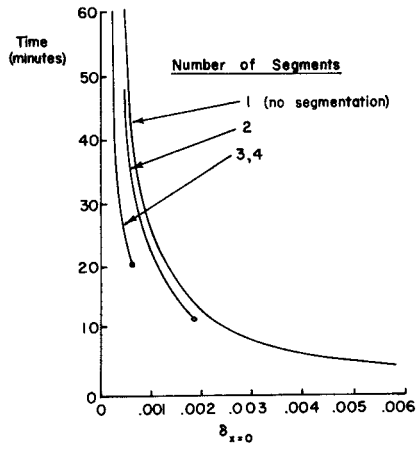

Fig. 5 Computation time for a typical calculation.

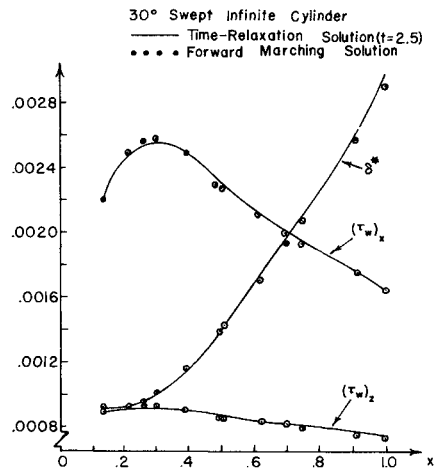

Fig. 6 Comparison of time-relaxation results with forward-marching results for a 30° swept infinite cylinder.

For initial boundary-layer thicknesses smaller than this, the run times become excessive. To circumvent this problem, a scheme was developed for segmenting the integration domain whereby segments were chosen such that the t-step length increased by a factor of 3 from each segment to the next. The factor of 3 meant that the integration mesh in any one segment merged smoothly into that in the adjacent one upstream. Figure 5 shows that the scheme was successful in reducing the longest computer times, but it could not reduce the shorter ones because the growth of the boundary-layer thickness was usually insufficient to permit more than one or two segments.

IV. Asymptotic Results Compared with Forward-Marching Method

To qualify the accuracy of the computer program, sample calculations were carried out for both two-dimensional and swept infinite cylinder flowfields in the time-relaxation mode, in which the boundary conditions are held constant and a steady-state solution is approached asymptotically for "large" times. In practice, "large times" turned out to be 2.5 time units, where a unit is the time required for a fluid particle traveling with some defined characteristic velocity to move a distance of one chord length. The results were compared to solutions obtained by the more conventional forward-marching procedure and the correlation is at least as good as that obtained previously by Patel and Nash.[2]

Figures 6 and 7 show the results of a comparison between the two methods for the case of flow over an infinite yawed cylinder, where the chordwise pressure gradient ($\partial p/\partial x$) is favorable over the forward part of the cylinder and adverse over the rear. In Figs. 6 and 7, all lengths (x, y, δ^*) are made dimensionless by division by the chord length of the cylinder, velocities by division by Q_{e_o} (the freestream velocity at infinity), and shear stresses by division by $\rho Q_{e_o}^2$. Figure 6 shows the predicted chordwise variations of δ^*, τ_{w_x} and τ_{w_z}. The greatest discrepancies between the two solutions are 1.2% in τ_{w_x} (at $x = 0.26$) and 3.0% in δ^* (at $x = 1.0$). Figure 7 shows the predicted chordwise and spanwise velocity profiles at $x = 1$, and it is evident, again, that the two methods produce nearly identical solutions.

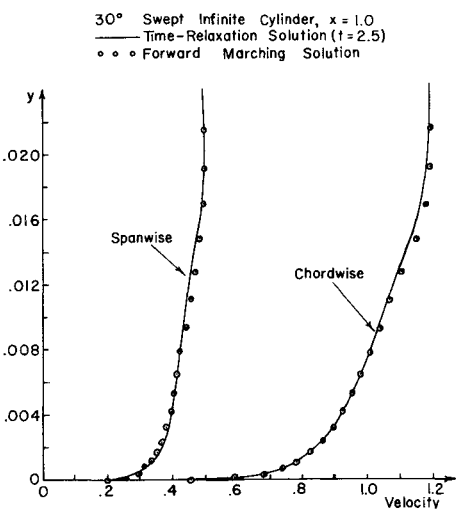

Fig. 7 Comparison of time relaxation velocity profiles with velocity profiles obtained via forward-marching method at the trailing edge of a 30° swept infinite cylinder.

V. Example Calculation of the Method

As an example of the utilization of the numerical method, a two-dimensional flowfield oscillating harmonically over a flat plate, according to the equation

$$U_e/U_{e_o} = 1 + A \sin \omega t \tag{13}$$

is considered. Quantities are made dimensionless as mentioned in Sec. IV. In addition, time is made dimensionless by multiplication by U_{e_o} (the freestream velocity at infinity and denoted Q_{e_o} in three-dimensional flow) and division by the length of the plate. The reduced frequency, ω, is defined as

$$\omega = 2\pi/P$$

where P is the period of the motion in time units. A is the constant amplitude.

The amplitude, A, and frequency ω, were varied over a reasonable range to determine their effects on the response of the turbulent boundary-layer characteristics to this oscillatory flowfield. The initial conditions for this calculation were taken to be the asymptotic steady-state solution obtained as time approaches infinity ($t = 2.5$ is sufficient) for $A = 0$. The boundary conditions for all time at the entrance station for the boundary layer ($x = 0$) were set by making $\delta_o \sim (U_e/U_{e_o})^{-0.2}$ and scaling the standard initial profiles accordingly. This condition, in fact, is just the requirement that the entrance conditions respond instantaneously to the edge velocity at any instant of time, i.e., quasi-steady conditions. The Reynolds number based on chord length (unity) was taken to be 10^7 and the initial boundary-layer thickness was 0.00444. The computer program was allowed to run a few time units ($t = 2$ seems to be sufficient) in order to let transients die out and the output was generated at several chord positions for several periods. Quasi-steady solutions were generated by selecting ωt = const and utilizing the forward-marching numerical method for steady-state flows.

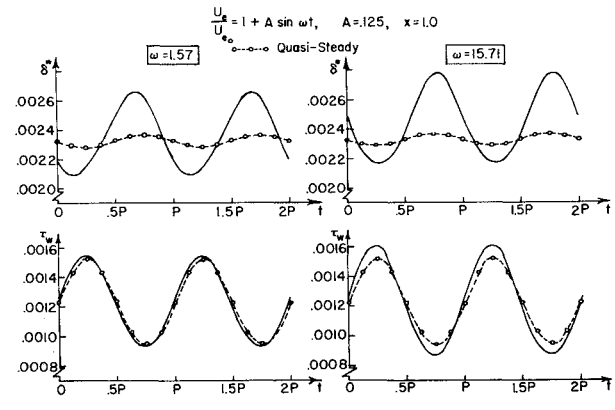

Fig. 8 Oscillatory flow over flat plate at low amplitude.

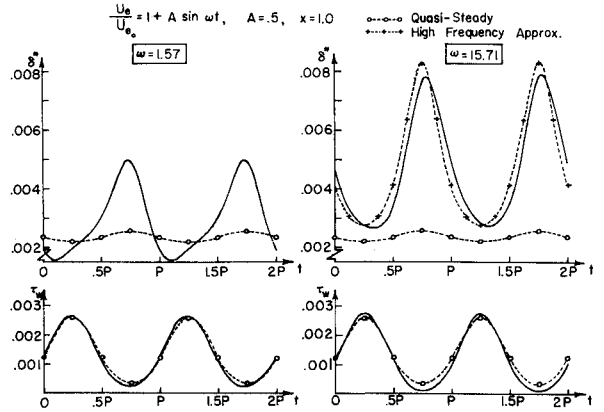

Fig. 9 Oscillatory flow over flat plate at high amplitude.

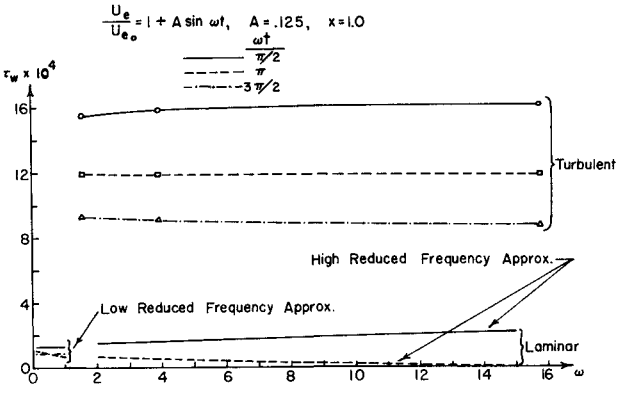

Fig. 11 Wall shear stress vs reduced frequency for laminar and turbulent flow.

Figure 8 shows the results for a ten-fold frequency range at an amplitude, A, of 12.5% and Fig. 9 shows the same frequency range at an amplitude of 50%. From Fig. 8, it is seen that the unsteady wall shear stress anticipates the quasi-steady values; i.e., there is a phase lead between wall shear stress and the external velocity, U_e. Similar effects have been predicted for oscillatory laminar boundary layers[12] and for perturbed turbulent boundary layers.[3]

At low frequencies, a phase lead is apparent in δ^* also; this phase lead decreases with increasing frequency, and at high frequencies the unsteady δ^* actually lags behind the quasi-steady values. The average level of δ^*, for the unsteady flow, increases with both increasing frequency and increasing amplitude, until the average unsteady δ^* is more than twice the average quasi-steady δ^* when $A_1 = 0.5$ and $\omega = 15.7$ (Fig. 9).

At 50% amplitude change (Fig. 9) the wall shear stress phase lead appears to decrease more with increasing frequency than at the lower amplitude. A peculiar skewing is seen in the δ^* curve although the shear stress remains symmetric about its mean value. Apparently, for this case the various states the turbulent boundary layer passes through at each instant of time due to a change in the external velocity are not reversible when the external velocity change is reversed. This situation is characteristic of flowfields approaching zero wall shear stress. The δ^* variation for the high frequency case in Fig. 9 can be approximately represented by a model in which the velocity profile moves in lock-step with the external flow. Such a model would be valid as $\omega \to \infty$, when $\partial U/\partial t$ would dominate the other terms in the equations of motion. This "high-frequency approximation" allows the statement, $U_e\delta^* = \text{const}$. This result is shown in Fig. 9, the constant having been determined for the best curve fit; it works equally well for the lower-amplitude case shown in Fig. 8. Whereas the displacement thickness is well represented by the high-frequency approximation, the wall shear stress continues to be well represented by the quasi-steady approximation, and it is remarkable that it works well over such a wide range of both frequency and amplitude.

Figures 10–13 show a comparison of the turbulent results with the laminar results of Lighthill.[12] In Fig. 10, a comparison is given of the laminar wall shear stress phase lead with the turbulent values vs the reduced frequency, ω. The turbulent wall shear stress phase lead is much reduced from the laminar values. Figure 11 shows a comparison of the laminar shear stress with the turbulent values vs reduced frequency, ω. Three curves are shown for each case corresponding to three values of the argument, ωt. The values for the high frequency approximation in the laminar case when $\omega t = \pi$ or $3\pi/2$ are identical and consequently are shown as only a dashed curve. Figures 12 and 13 give graphs of the displacement thickness values analogous to the Figs. 10 and 11. From these figures, it is seen

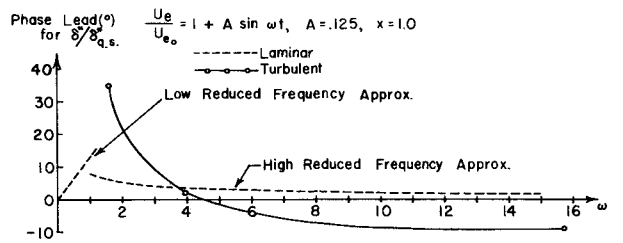

Fig. 12 Displacement thickness phase lead vs reduced frequency for laminar and turbulent flow.

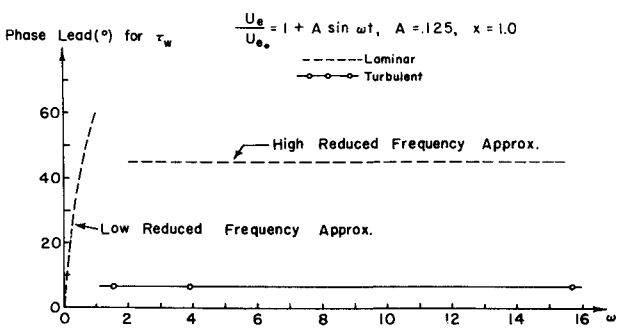

Fig. 10 Wall shear stress phase lead vs reduced frequency for laminar and turbulent flow.

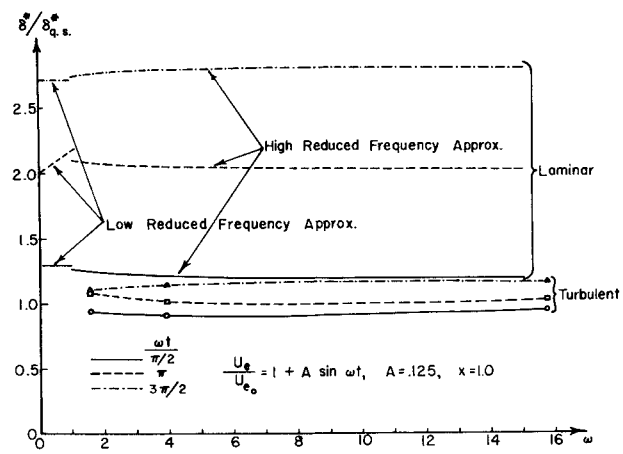

Fig. 13 Displacement thickness vs reduced frequency for laminar and turbulent flow.

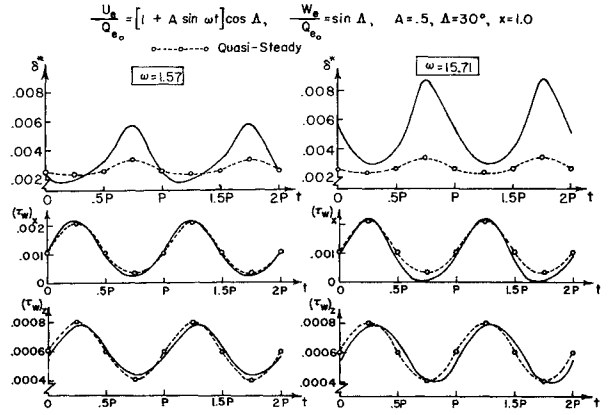

Fig. 14 Oscillatory flow over 30° swept flat plate at high amplitude.

that the turbulent boundary-layer results display the same trends as in the laminar case.

In the laminar case the phase lead increases with frequency, up to a maximum of $\pi/4$. In the present results, however, the phase lead is considerably smaller than this (see Fig. 10). The phase leads predicted here are also smaller than the values calculated by McDonald and Shamroth.[3] Their results may have been compromised by inadequacies in the velocity-profile model used in their integral method, and the disagreement may not put the validity of the present results in question.

A variation of the flow given by Eq. (13) is that of a swept infinite flat plate immersed in a flow oscillating harmonically in the chordwise direction only, according to the equations

$$U_e/Q_{e_o} = [1 + A \sin \omega t] \cos \Lambda$$

$$W_e/Q_{e_o} = \sin \Lambda$$

where Q_{e_o} is the velocity magnitude at $t = 0$ and Λ is the sweep angle. Results of this calculation are shown in Fig. 14 for 50% amplitude change. The curves for δ^* and $(\tau_w)_x$ have the same characteristics as in the two-dimensional case with the exception of the skewing of the chordwise wall shear stress at the higher frequency value. This result is probably accentuated by the closeness of the chordwise wall shear stress to zero. However, the spanwise wall shear stress, in contrast to the chordwise wall shear stress, lags the quasi-steady values and this phase lag apparently increases with increasing frequency.

In conclusion, it has been shown that, even though a very simply unsteady freestream flow example was chosen, there can be significant unsteady flow effects on the turbulent boundary layer. This is particularly true in the case of the boundary-layer displacement thickness which exhibited significant unsteady effects to the lowest frequency considered. Even more remarkable results are obtained when the calculations are made for flows with adverse pressure gradients.[6,7]

References

[1] Hicks, J. G. and Nash, J. F., "The Calculation of Three-Dimensional Turbulent Boundary Layers on Helicopter Rotors," CR-1845, May 1971, NASA.

[2] Patel, V. C. and Nash, J. F., "Some Solutions of Unsteady Turbulent Boundary Layer Equations," *Proceedings of the IUTAM Symposium on Unsteady Boundary Layers,* Quebec, Canada, 1971, pp. 1106–1164.

[3] McDonald, H. and Shamroth, S. J., "An Analysis and Application of the Time-Dependent Turbulent Boundary-Layer Equations," *AIAA Journal,* Vol. 9, No. 8, Aug. 1971, pp. 1553–1560.

[4] Bradshaw, P., "Calculation of Boundary Layer Development Using the Turbulent Energy Equation. VI Unsteady Flow," NPL Aero Rept. 1288, Feb. 1969, National Physics Lab., England.

[5] Abbott, D. E. and Cebeci, T., "The General Analysis of Unsteady Boundary Layers—Laminar and Turbulent," In *Fluid Dynamics of Unsteady, Three-Dimensional and Separated Flows, Proceedings of a Project SQUID Workshop,* edited by F. J, Marshall, Georgia Institute of Technology, Atlanta, Ga., 1971.

[6] Nash, J. F., Carr, L. W., and Singleton, R. E., "Unsteady Turbulent Boundary Layers in Two-Dimensional, Incompressible Flow," AIAA Paper 73-650, Palm Springs, Calif., 1973.

[7] Singleton, R. E., Nash, J. F., Carr, L. W., and Patel, V. C., "Unsteady Turbulent Boundary-Layer Analysis," TM X-62, 242, Feb. 1973, NASA.

[8] Nash, J. F. and Patel, V. C., "A Generalized Method for the Calculation of Three-Dimensional Turbulent Boundary Layers," in *Fluid Dynamics of Unsteady, Three-Dimensional and Separated Flows, Proceedings of a Project SQUID Workshop,* edited by F. J. Marshall, Georgia Institute of Technology, Atlanta, Ga.,1971.

[9] Nash, J. F. and Patel, V. C., *Three-Dimensional Turbulent Boundary Layers,* SBC Technical Books, Atlanta, Ga., 1972.

[10] Nash, J. F., "An Explicit Scheme for the Calculation of Three-Dimensional Turbulent Boundary Layers," *Journal of Basic Engineering,* March 1972, pp. 131–141.

[11] Townsend, A. A., "Equilibrium Layers and Wall Turbulence," *Journal of Fluid Mechanics,* Vol. 11, Pt. 1, Aug. 1961, p. 97.

[12] Lighthill, M. J., "The Response of Laminar Skin Friction and Heat Transfer to Fluctuations in the Stream Velocity," *Proceedings of the Royal Society A224,* 1954, p. 1.